Proceedings of the 2018 IEEE/ASME International
Conference on Advanced Intelligent Mechatronics (AIM),
Auckland, New Zealand, July 9-12, 2018

Continuum Delta Robot: a Novel Translational Parallel Robot with Continuum Joints

Zhixiong Yang, Xiangyang Zhu, *Member, IEEE*, and Kai Xu*, *Member, IEEE*

***Abstract*—Researches on continuum robots thrive due to many advantages such as design compactness and motion dexterity. Among the recent advances, it is well noted the proposal of Parallel Continuum Robot (PCR) whose legs are made from elastic rods. The legs undergo deformations along their entire lengths and sophisticated mechanics is used to describe their shapes and the kinematics. Following a different approach, this paper proposes to design parallel robots with continuum joints. The continuum joints would assume constant curvature bending and hence produce relatively simple kinematics. With the bending ranges achievable beyond 90°, a parallel robot with continuum joints, instead of universal or spherical joints, can realize larger workspace. As a particular demonstrative example, a Continuum Delta Robot (CDR) is proposed. Each of the CDR's legs consists of two coupled continuum joints which inherently realize translational movements of the end effector. The design concept, kinematics, system description and experimental characterizations are presented. From the presented Continuum Delta Robot, more parallel robots with continuum joints can be proposed and new design methodology can be developed.**

I. Introduction

Continuum robots, a term coined in [1], attracted a lot of attentions in the past a few decades due to many advantages, such as inherent safety, structural simplicity, design compactness, as well as motion dexterity in confined spaces [2]. Via intrinsic, extrinsic or hybrid actuation [1], a continuum robot deforms itself to realize motion and manipulation. Its kinematics then depends on the deformed shapes (e.g., bending with possible extension/contraction). An approximation in the kinematics modeling assumes that the deformed portion (usually called a segment or a section) undergoes constant curvature bending [3]. This assumption is experimentally verified [4] and widely considered acceptable while gauged by the exact deforming shapes of the continuum segments that are obtained using iteratively solved nonlinear mechanics [5], elliptic integrals [6], Cosserat rod theory [7], virtual power [8], etc.

Continuum robots have found considerable applications in medical robotic systems [9], and industrial inspection, grasping, manipulation and even locomotion [10-16]. In many of the aforementioned examples, the applied continuum robots either possess a few serially connected segments for enhanced mobility and dexterity, or have several segments connected to a base in parallel for grasping or locomotion. Under the constant curvature bending assumption, each segment usually possesses two bending DoFs (Degrees of Freedom). Alternatively, multi-DoF movements could also be realized by a recently proposed PCR (Parallel Continuum Robot) that is similar to a Gough-Stewart parallel robot [17, 18], as shown in Fig. 1(a). Accurate positioning and dexterous orientating of the moving platform is achieved by the deformed legs. Cosserat rod theory was used to describe the deformed shapes and kinematics. However, computational efficiency [19] of the sophisticated mechanics model and elastic stability [20] of the elastic legs could seem daunting when one attempts to build his/her own PCR.

Aiming at expanding the boundaries of continuum robotics research, this paper proposes to design parallel robots with continuum joints. The continuum joints would assume constant curvature bending and hence produce simpler kinematics than the PCR whose legs are made from thin rods and the kinematics model relies on the Cosserat rod theory. Furthermore, these continuum joints possess two more characteristic features: i) large motion ranges, and ii) easily realizable coupling between two such joints.

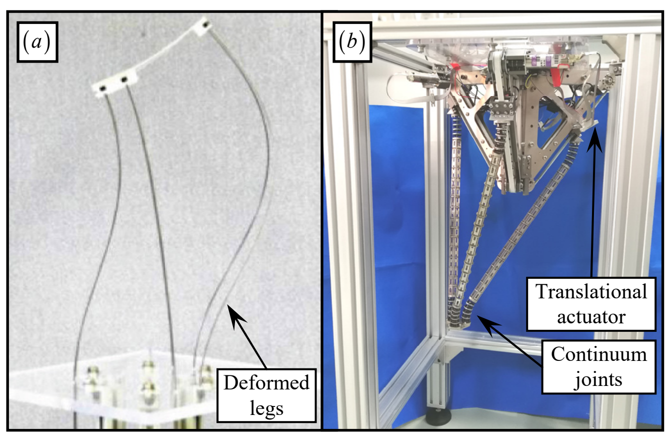

Fig. 1. Non-rigid parallel robots: (a) the Stewart-type PCR in [17], and (b) the proposed CDR (Continuum Delta Robot)

In this paper, a Continuum Delta Robot (CDR) is proposed as a demonstrative example, as shown in Fig. 1(b). Each of the CDR's legs consists of two coupled continuum joints which inherently realize translational movements of the moving platform.

Manuscript received Feb 19*th*, 2018. This work is supported in part by the National Natural Science Foundation of China (Grant No. 51722507, Grant No. 51435010 and Grant No. 91648103), and in part by National Key R&D Program of China (Grant No. 2017YFC0110800).

Zhixiong Yang is with the RII Lab (Lab of Robotics Innovation and Intervention), UM-SJTU Joint Institute, Shanghai Jiao Tong University, Shanghai, China (e-mail: yangzhixiong@sjtu.edu.cn).

Kai Xu and Xiangyang Zhu are with the State Key Laboratory of Mechanical System and Vibration, School of Mechanical Engineering, Shanghai Jiao Tong University, Shanghai, China (asterisk indicates the corresponding author, phone: +86-21-34206547; emails: k.xu@sjtu.edu.cn and mexyzhu@sjtu.edu.cn).

978-1-5386-1854-7/18/$31.00 ©2018 IEEE

The proposed CDR is actuated by three translational actuators and possesses three DoFs under the constant curvature bending assumption of the continuum joints. This assumption, which leads to the CDR's simple kinematics, would be verified by the to-be-presented experimental results achieving ±0.5 mm positioning accuracy.

If a continuum joint is designated as a C joint, the proposed CDR is a 3-PCC parallel robot. The existing counterparts include the 3-PSS robot (the linear Delta robot) [21] and the 3-PUU robots [22-24]. With the bending ranges possibly achievable beyond ±90° as indicated in Fig. 2(a), the parallel robot with continuum joints, instead of universal or spherical joints, can realize larger workspace.

The CDR's parallel structure realizes its stiffness of about 4 N/mm in the XY directions and about 57 N/mm in the Z direction. This stiffness level could be beneficial in maintaining an acceptable positioning accuracy as well as avoiding damaging delicate workpieces if the CDR is applied in pick-and-place tasks. Existing researches on parallel robots regarding their compliance mostly focus on the actuator/joint compliance [25] and the links' flexibility (e.g., in [26]).

Flexure joints in parallel robots (e.g., in [27-32]) can be seen similar to the continuum joints. The core differences are summarized as follows. Firstly, a continuum joint inherently possesses two bending DoFs under the constant curvature bending assumption where twisting is neglected. Then the rod-type flexure joint is most comparable. But the allowed bending range of a continuum joint could be beyond ±90° as shown in Fig. 2(a) and [6], which might be substantially larger than that of a rod-type flexure joint. Secondly, a continuum joint assumes a circular arc shape with a non-negligible length. On the other hand, a rod-type flexure joint is either approximated as a universal joint (even a spherical joint in some cases) or undergoes small deflection as an Euler-Bernoulli beam. Most uniquely, motions of two continuum joints in a parallel robot can be coupled by connecting their structural members (e.g., the backbones as explained in Section II). Then two coupled joints can produce a translational motion which is only realized by a parallelogram with four joints (flexure or spherical).

The core contributions of this paper lie on the proposal of parallel robots with continuum joints. To illustrate the distinctive features the continuum joints can bring, the design concept, kinematics, system descriptions and experimental characterizations of a Continuum Delta Robot is presented. To the best of the authors' knowledge, the proposed CDR is the first parallel robot with continuum joints. It is expected that more parallel robots with continuum joints can be proposed from the CDR and new design methodology can be developed.

This paper is organized as follows. Section II explains the design concept while Section III presents the kinematics and dimension optimization. The CDR's system descriptions are detailed in Section IV with the kinematic calibrations and the experimental characterizations reported in Section V. Section VI summarizes the conclusions and the future work.

II. Design Concept

A continuum joint in a parallel robot consists of an end disk, a few spacer disks and several backbones made from super-elastic nitinol, as shown in Fig. 2(b). Each backbone is fixed at the end disk and can slide in the holes of the spacer disks and inside the multi-lumen tube. When an external wrench is exerted on the end disk, the continuum joint would be bent and the backbones would generate translational movements inside the multi-lumen tube.

If two identical sized continuum joints are coupled by connecting their corresponding backbones inside the multi-lumen tube as shown in Fig. 2(b), it forms a particular case of a dual continuum mechanism that was proposed in [33]. Then the two continuum joints are addressed as the Proximal Joint (PJ) and the Distal Joint (DJ). The PJ's bending will bend the DJ in the opposite direction for the same amount due to the fact that translational movements of the PJ's backbones push and pull the DJ's backbone to bend the DJ. Detailed proof should be referred to the backbone actuation kinematics for a dual continuum mechanism as in [33]. In a practical implementation, the corresponding backbones of the PJ and the DJ are physically one piece, routed from the DJ to the PJ.

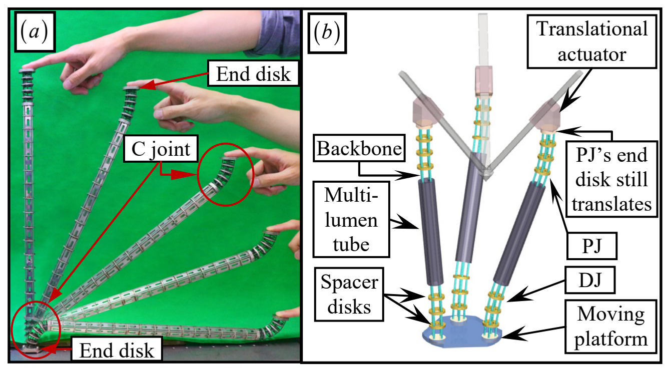

Fig. 2. Design concept: (a) bending shapes of a leg with two coupled continuum joints, and (b) the proposed CDR

When the PJ and the DJ undergo the same amount of bending in the opposite direction, the end disk of the DJ will always be parallel to that of the PJ. Then a pair of coupled PJ and DJ with the connecting multi-lumen tube form one of the three legs of the Continuum Delta Robot as in Fig. 2(b).

Three linear guide actuators translate the PJ's end disks of the three legs, while the three DJ's end disks are attached to a moving platform. Translations of the moving platform are hence realized under the motion constraint that the DJ's end disk always translates with respect to the PJ's end disk. This actuation is different from the conventional way of actuating a continuum robot: none of the backbones is directly actuated.

Using C to designate a continuum joint, the proposed CDR is a 3-PCC parallel robot. In a sense, it is similar to a 3-PSS linear Delta robot with inclined guideways (e.g., the Keops robot in [21]). Other existing counterparts include the 3-PUU robots [22-24]. The use of the continuum joints allows bigger joint motion ranges: ±90° for a continuum joint v.s. ±30° for a spherical joint as in [21] and ±20° for the cone angle limit of a universal joint as in [24]. What's more, the coupling between the DJ and the PJ replaces the parallelogram in a Delta robot to produce translational outputs.

III. Kinematics

When the three end disks of the legs' proximal joints are translated by the linear guide actuators, all the continuum joints bend passively. Translations of the moving platform are realized under the motion constraint imposed by the coupling between the DJ and the PJ.

The CDR's pose/kinematics is determined by the minimum of the robot's potential energy (including gravitational and elastic portions). Under the CDR's installation orientation, each leg will have lower gravitational and elastic potential energies with less bending. Under the same bending angle, the DJ and the PJ will have lower elastic potential energy for the constant curvature bending. The CDR has six continuum joints that are connected. Their potential energies can be redistributed passively to reach a minimum. Hence it is approximated that the DJs and the PJs all undergo constant curvature bending. This modeling assumption is widely adopted [3] and experimentally validated [6]. The experimental results presented in Section V also verify the validity of this assumption.

Nomenclature and several coordinate systems are defined in Section III.A, while the inverse kinematics is derived in Section III.B. A dimension optimization is then presented in Section III.C.

A. Nomenclature and Coordinate Systems

Nomenclature is defined in Table I, while the assigned coordinate systems are defined as follows, referring to Fig. 3 and Fig. 4.

TABLE I
Nomenclature Used in Kinematics Modeling

Symbol	Representation
i	Index of the CDR's legs, $i=1,2,3$
α_i	Axis inclination angle of the guideway in the ith leg
β_i	$\beta_i=(i-1)\pi/3$ is the division angle from $\hat{\mathbf{x}}_0$ to the projection of the ith guideway actuator's axis on the XY plane of $\{O\}$.
q_i	q_i is the actuation length of the ith leg, measured from the origin O to the center of the PJ's end disk along the guideway actuator's axis.
L_i	Length of the PJ and the DJ in the ith leg
D_i	Length of the straight multi-lumen guiding tube in the ith leg
θ_i	Bending angle of the PJ and the DJ in the ith leg
δ_i	A right-handed rotation angle from $\hat{\mathbf{y}}_{i1}$ to $\hat{\mathbf{x}}_{ipe}$ about $\hat{\mathbf{z}}_{ipe}$.
ϕ_i	$\phi_i=(i-1)\pi/3$ is the division angle from $\hat{\mathbf{x}}_P$ to a ray passing through the center of the DJ's end disk in the ith leg.
r_i	Distance from the origin P to the center of the DJ's end disk in the ith leg.

- *Reference Coordinate* $\{O\}\equiv\{\hat{\mathbf{x}}_0,\hat{\mathbf{y}}_0,\hat{\mathbf{z}}_0\}$ locates its origin O at the intersection of three axes along which the PJ's end disk is translated. The $\hat{\mathbf{x}}_0$ points towards the *1*st leg.
- *End disk Coordinate of the ith PJ* $\{ipe\}\equiv\{\hat{\mathbf{x}}_{ipe},\hat{\mathbf{y}}_{ipe},\hat{\mathbf{z}}_{ipe}\}$ is fixed to the center of PJ's end disk in the ith leg, translated from $\{O\}$.
- *Bending Plane Coordinate 1 of the ith leg* $\{i1\}\equiv\{\hat{\mathbf{x}}_{i1},\hat{\mathbf{y}}_{i1},\hat{\mathbf{z}}_{i1}\}$ shares its origin with $\{ipe\}$. $\hat{\mathbf{x}}_{i1}$ is aligned with $\hat{\mathbf{z}}_{ipe}$ such that the ith leg bends in the XY plane of $\{i1\}$.
- *Bending Plane Coordinate 2 of the ith leg* $\{i2\}\equiv\{\hat{\mathbf{x}}_{i2},\hat{\mathbf{y}}_{i2},\hat{\mathbf{z}}_{i2}\}$ is translated from $\{i1\}$ with the origin located at the center of the DJ's end disk.

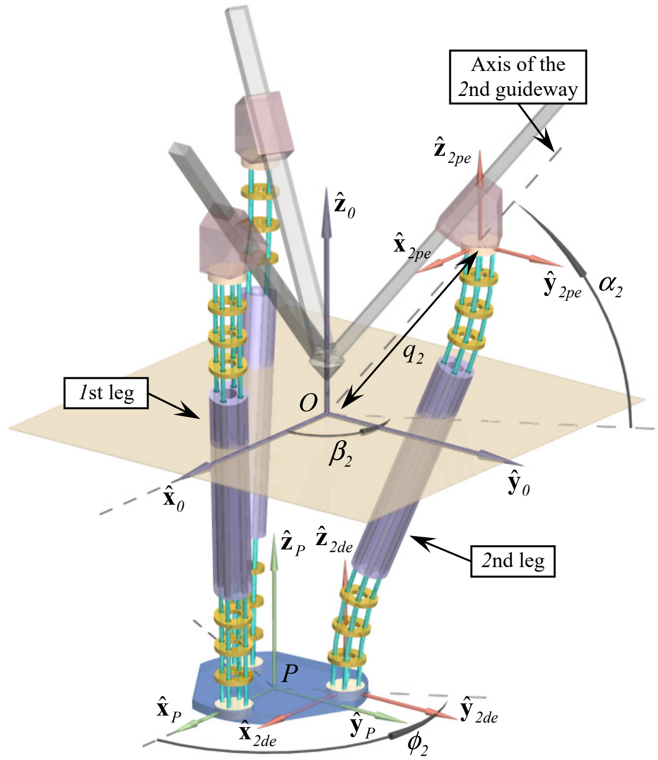

Fig. 3. Nomenclature and coordinates of the CDR

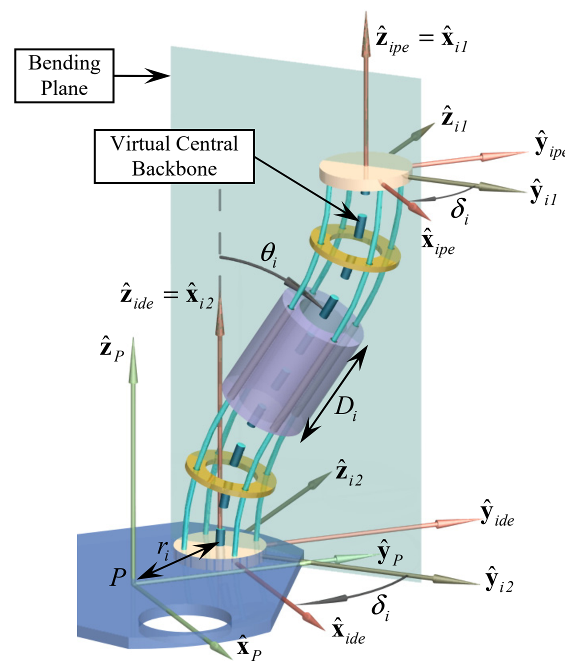

Fig. 4. Nomenclature and coordinates of the ith leg

- *End Disk Coordinate of the ith DJ* $\{ide\}\equiv\{\hat{\mathbf{x}}_{ide},\hat{\mathbf{y}}_{ide},\hat{\mathbf{z}}_{ide}\}$ is attached to the center of the DJ's end disk in the ith leg. The coupled bending of the DJ and the PJ maintains the same orientation between $\{i1\}$ and $\{i2\}$, $\{ipe\}$ and $\{ide\}$, respectively.

- *Moving Platform Coordinate* $\{P\} \equiv \{\hat{\mathbf{x}}_P, \hat{\mathbf{y}}_P, \hat{\mathbf{z}}_P\}$ locates its origin P at the center of the end platform, translated from $\{ide\}$. Please note that all the $\{ide\}$ coordinates and the $\{ipe\}$ ones have the same orientation since only translational motions are generated on the moving platform. The $\hat{\mathbf{x}}_P$ points towards the *1*st leg.

B. Inverse Kinematics

For a parallel robot, it is often more convenient to start with the inverse kinematics. The CDR's forward kinematics (like the one solved for a Gough-type parallel manipulator [34]) will be deferred to a future study where all the respects for the CDR's kinematics will be investigated.

The position of the center of the moving platform ${}^{O}\mathbf{p}_P = [x_P\ y_P\ z_P]^T$ in $\{O\}$ is of interest.

The end disk of the DJ in the ith leg is fixed to the moving platform and the homogeneous transformation matrix linking $\{P\}$ and $\{ide\}$ can be written as in (1).

$$ {}^{ide}\mathbf{T}_P = \begin{bmatrix} \mathbf{I}_{3\times 3} & {}^{ide}\mathbf{p}_P \\ \mathbf{0} & 1 \end{bmatrix} \tag{1} $$

Where ${}^{ide}\mathbf{p}_P = r_i\,[\cos\phi_i\ \sin\phi_i\ 0]^T$.

The homogeneous transformation matrix linking $\{ide\}$ and $\{ipe\}$ is written as in (2). Since the DJ and the PJ within the ith leg always undergo the same amount of bending in the opposite direction, $\{ide\}$ is translated from $\{ipe\}$. The path for this translation can be characterized by a virtual central backbone as the dashed line in Fig. 4, within the bending plane that is characterized by δ_i. The entire virtual central backbone consists of three sequential portions: i) the PJ's central backbone (a circular arc of length L_i and bent angle θ_i); ii) the axis of the multi-lumen tube for a distance of D_i; and iii) the DJ's central backbone (again a circular arc of length L_i and bent angle θ_i). The expression of ${}^{ipe}\mathbf{p}_{ide}$ is derived in (3).

$$ {}^{ipe}\mathbf{T}_{ide} = \begin{bmatrix} \mathbf{I}_{3\times 3} & {}^{ipe}\mathbf{p}_{ide} \\ \mathbf{0} & 1 \end{bmatrix} \tag{2} $$

$$ {}^{ipe}\mathbf{p}_{ide} = \begin{bmatrix} 2L_i(\cos\theta_i - 1)\cos\delta_i/\theta_i - D_i\sin\theta_i\cos\delta_i \\ 2L_i(1-\cos\theta_i)\sin\delta_i/\theta_i + D_i\sin\theta_i\sin\delta_i \\ -2L_i\sin\theta_i/\theta_i - D_i\cos\theta_i \end{bmatrix} \tag{3} $$

Where ${}^{ipe}\mathbf{p}_{ide} = [0\ 0\ 2L_i{+}D_i]^T$ when θ_i approaches zero, using the Taylor expansion of $\sin\theta_i$ and $\cos\theta_i$.

The guideway actuator translates the PJ's end disk along its axis that passes the origin O. Then the homogeneous transformation linking $\{O\}$ and $\{ipe\}$ is written in (4).

$$ {}^{O}\mathbf{T}_{ipe} = \begin{bmatrix} \mathbf{I}_{3\times 3} & {}^{O}\mathbf{p}_{ipe} \\ \mathbf{0} & 1 \end{bmatrix} \tag{4} $$

Where ${}^{O}\mathbf{p}_{ipe} = q_i[\cos\beta_i\cos\alpha_i\ \ \sin\beta_i\cos\alpha_i\ \ \sin\alpha_i]^T$.

With ${}^{O}\mathbf{T}_{ipe}$, ${}^{ipe}\mathbf{T}_{ide}$ and ${}^{ide}\mathbf{T}_P$ derived, the kinematics for ${}^{O}\mathbf{p}_P$ concerning the ith leg is formulated in (5).

$$ \begin{bmatrix} {}^{O}\mathbf{p}_P & 1 \end{bmatrix}^T = {}^{O}\mathbf{T}_P \begin{bmatrix} \mathbf{0}_{1\times 3} & 1 \end{bmatrix}^T \tag{5} $$

Where ${}^{O}\mathbf{T}_P = {}^{O}\mathbf{T}_{ipe}\,{}^{ipe}\mathbf{T}_{ide}\,{}^{ide}\mathbf{T}_P$ is a function of θ_i, δ_i and q_i, given the structural parameters of α_i, β_i, L_i, D_i, r_i and ϕ_i.

A point at ${}^{O}\mathbf{p}_P = [x_P\ y_P\ z_P]^T$ is admitted into the CDR's workspace, when the kinematics in (5) is solvable for a set of θ_i, δ_i and q_i values within their joint ranges (e.g., $\theta_i \in [0°, 90°]$, $\delta_i \in (-180°, 180°]$ and $q_i \in [50\text{mm}, 300\text{mm}]$), for each leg of the CDR. The inverse kinematics in (5) was solved using the Newton-Raphson method in MATLAB. $\mathbf{q} = [q_1\ q_2\ q_3]^T$ is the joint space vector, while θ_i and δ_i are intermediate variables to determine the poses of each leg.

C. Dimension optimization

With the kinematics of the CDR derived, a dimension optimization for maximizing the CDR's workspace was carried out to determine the CDR's structural parameters.

There are six structural parameters in the CDR: α_i, β_i, L_i, D_i, r_i and ϕ_i. For the sake of simplicity, $\beta_i = \phi_i = (i-1)\pi/3$, while α_i, L_i, r_i and D_i are set identical for all the three legs.

Since the optimization tries to maximize the CDR's workspace, it is obvious that the longer the legs are, the bigger workspace will be obtained. Hence a constraint is set in (6).

$$ L_i + D_i = 500\ \text{mm} \tag{6} $$

It is desired that the CDR would possess an acceptable stiffness. It is known that a longer continuum joint would lead to a lower stiffness of this joint. Hence the optimization is set as in (7), where $\alpha = \alpha_1 = \alpha_2 = \alpha_3$ is the inclination angle of the actuator guideway, $L = L_1 = L_2 = L_3$ is the length of the continuum joint, $r = r_1 = r_2 = r_3$ is the radius for the DJs' distribution, and V_{CDR} is the volume of the CDR's workspace that is obtained when $\theta_i \in [0, 90°]$, $\delta_i \in (-180°, 180°]$ and $q_i \in [50\text{mm}, 300\text{mm}]$ by scanning the joint space $\mathbf{q}$.

$$ \max_{\alpha, L, r} \frac{V_{CDR}}{L} \tag{7} $$

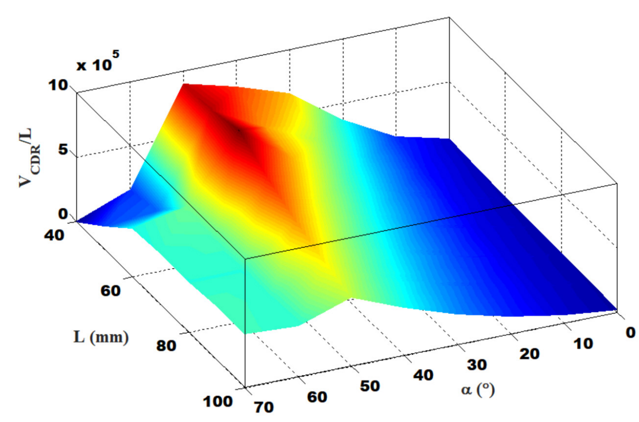

Fig. 5. Dimension optimization for the CDR when $r = 20$ mm

The optimization was conducted in an enumerative manner by varying α, L and r in increments of 10° and 10mm from 0° to 70°, from 40 mm to 100 mm, and from 20 mm to 50 mm, respectively. The maximum is reached at $\alpha = 50°$, $L = 60$ mm and $r = 20$ mm. And these three values were assigned to the structure of the CDR. The plot in Fig. 5 is for r = 20 mm, due to the difficulty in visualizing the optimization value for three variables.

Using the structural and actuator parameters of the CDR listed in Table II, the CDR's workspace can be visualized in Fig. 6 with a CDR's pose shown. If the joint limit on θ_i is reduced to 30°, the workspace would be substantially reduced to about 26.1% of the original volume, as in Fig. 6 as well.

TABLE II
Parameters of the CDR

$\alpha_i = 50°$	Li = 60 mm	r_i = 20 mm	D_i = 380 mm
$\beta_1 = \phi_1 = 0°$	$\beta_2 = \phi_2 = 120°$	$\beta_3 = \phi_3 = 240°$	
$\theta_i \in [0°,90°]$	$\delta_i \in (-180°,180°]$	$q_i \in$ [50mm, 300mm]	

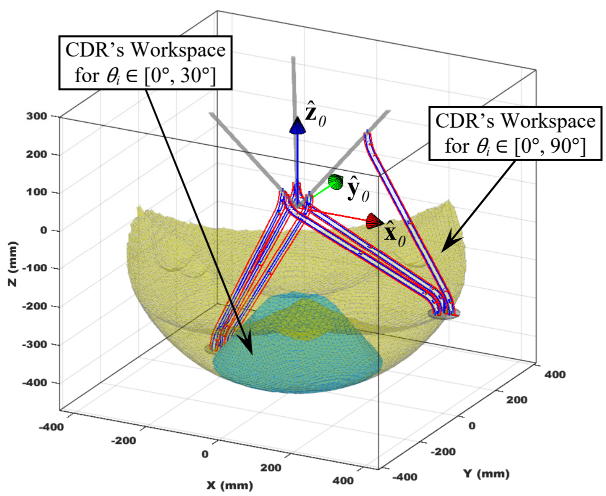

Fig. 6. Workspace of the CDR

IV. System Descriptions of the CDR

With the kinematics and dimensional optimization of the CDR carried out in Section III, detailed system descriptions are described in this section.

A. Structure of CDR

The CDR consists of three identical legs with two coupled continuum joints, as shown in Fig. 7. Within each leg, a Ø22mm multi-lumen tube is used to connect the DJ and the PJ with the same outer diameter. To reduce tooling cost and weight, this multi-lumen tube is fabricated by welding multiple spacer disks and strips to four stainless steel tubes using a laser welding machine.

Backbones of the continuum joints are arranged around a Ø20mm circle, routed from the DJ to the PJ through the channels of the multi-lumen tube.

The backbones are made from super-elastic nitinol, whose elastic strain range can be as high as 6 ~ 8 % [35]. In order to achieve a proper safety factor, a maximum of 2% strain is allowed. Due to the material availability that is in stock, the backbones are set to have a diameter of 1.2mm. The maximal strain is about 1.6% for a 90° bending on the joint.

All the CDR's three legs are attached to the moving platform. The centers of the DJ's end disks are evenly distributed on a Ø40 mm circle (a.k.a., r_i = 20 mm).

The PJ's end disks are attached to the sliders of three guideway actuators, via connection wedges. In inclination angle of the guideway actuators is 50°. Via the connection wedges, the PJ's end disks are kept at horizontal orientation during translations.

Each of the guideway actuators consists of a motor, a timing belt assembly, a linear rail and a slider. The motors (DCX22L) with the GPX-22 gearheads (gear ratio of 21:1) are from Maxon Inc. Three limit switches (EE-SX672 from OMRON Inc.) are mounted on the linear rails for actuator homing.

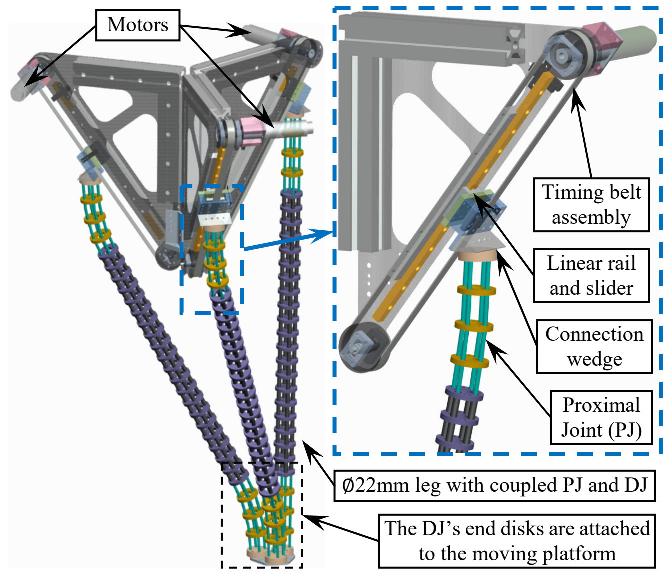

Fig. 7. Structure of the CDR

B. Control Infrastructure

The CDR's control infrastructure is mostly designed for the proof-of-concept experiments.

An embedded controller (Apalis T30 from Toradex AG, Switzerland) with a 1.3GHz multi-core CPU and 1GByte RAM is chosen as the central controller. It comes with an operating system that is based on Linux and customized for Apalis T30.

Three digital drivers (EPOS 24/2 from Maxon Inc.) are used to drive the motors. The driver communicates with the central controller via the CAN (Controller Area Network) bus according to the standard CANopen protocol. One digital I/O of the driver is connected to the limit switch of the linear guideway actuator for homing operation.

V. Experimental Characterizations

After the CDR constructed, a series of experiments were carried out to characterize its performance.

A. Calibrations and Actuation Compensation

Since the continuum joints (PJ and DJ) passively bend into circular arcs, existing compensation methods in [36, 37] that realizes accurate bending angles are not required. Instead, the implemented calibration refers to an existing approach for a Delta robot as in [38].

The presented calibration focuses on the CDR's structure parameters whose errors come from various aspects, such as fabrication and assembling. 21 parameters of the three legs are involved, as listed in Table III. All the parameters except q_{i_home} are designed according to the dimensional optimization results. q_{i_home} is the position of the limit switch for homing.

For the motion calibration, the CDR was commanded to move to 96 positions inside its workspace three times. The 96 positions are evenly distributed on four circles with the diameters of 150mm and 300mm and the centers located at $[0\ 0\ -300\text{mm}]^T$ and $[0\ 0\ -350\text{mm}]^T$ in $\{O\}$. The actual positions of the moving platform were recorded using an optical tracker (Micron Tracker SX60 from Claron Tech Inc) via the three markers placed on the moving platform and two markers perpendicularly placed on the CDR's base, as shown in Fig. 8.

The calibration is carried out as an optimization as formulated in (8). The *fminunc* function in MATLAB was used to solve this optimization, using the nominal structural values as the initial guesses. The results, as the actual structural values, are obtained and listed in the Table III.

$$[\alpha_i,\beta_i,\phi_i,L_i,D_i,r_i,q_{i\_home}] = \operatorname{argmin}\sum\left\| {}^{O}\tilde{\mathbf{P}}_{measured} - {}^{O}\mathbf{T}_{ipe}\,{}^{ipe}\mathbf{T}_{ide}\,{}^{ide}\mathbf{T}_{P}[0\ \ 0\ \ 0\ \ 1]^T \right\| \tag{8}$$

Where ${}^{O}\tilde{\mathbf{P}}_{measured} = \left[{}^{O}\mathbf{P}^T_{measured}\ \ 1\right]^T$ is the homogeneous vector for the measured positions of the moving platform in $\{O\}$.

TABLE III
Calibrated Parameters of the CDR

Leg index	α_i (°)	β_i (°)	ϕ_i (°)	L_i (mm)	D_i (mm)	r_i (mm)	q_{i_home} (mm)
1	51.28	0.03	-0.01	60.00	390.00	19.99	314.13
2	50.90	119.98	120.01	59.97	384.98	20.01	314.69
3	51.83	239.99	240.00	60.02	390.00	19.99	314.17

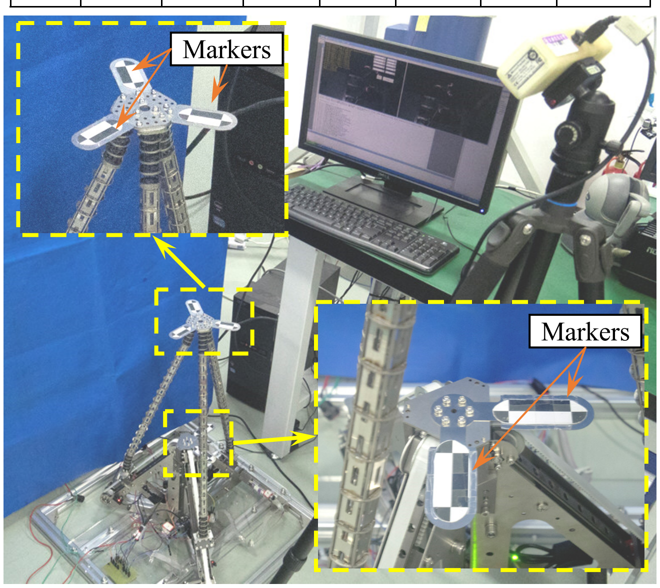

Fig. 8. Experimental setup for the motion calibration

Then the CDR was instructed to reach the same and 24 additional positions to verify the calibration. The positioning errors before and after the calibration for the first 96 positions are presented in Fig. 9. The errors are reduced to ±0.5mm on the Ø150mm circle and ±1 mm on the Ø300mm circle whose centers are both located at $[0\ 0\ -300\text{mm}]^T$ in $\{O\}$.

The 24 additional positions are distributed on the vertices of six squares with the edge lengths of 100 mm, 200 mm, and 300mm, and the centers at $[0\ 0\ -240\ \text{mm}]^T$ and $[0\ 0\ -340\ \text{mm}]^T$ in $\{O\}$, respectively, as shown in the inset of Fig. 10. The positioning errors are plotted in Fig.10.

The positioning errors for points further away from the origin of $\{O\}$ become larger, because the continuum joints in the CDR bend more under these poses. Then the internal wrench interactions between the continuum joints and other structural members might have deviated the continuum joints from their assumed circular shapes, leading to increased errors. It is desired to improve the motion calibration results in a future study, via using more sophisticated approaches (e.g., the iterative algorithm in [39] or taking the measurement errors into consideration as in [40]).

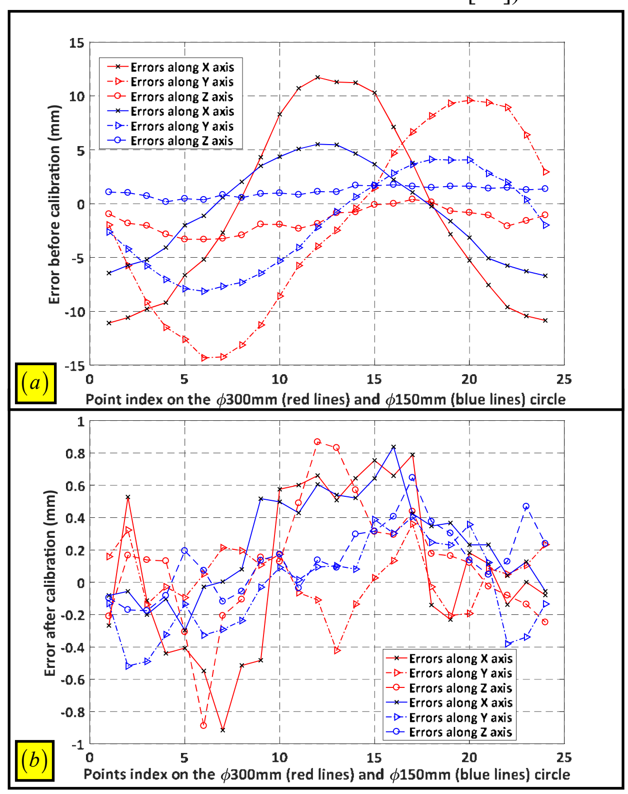

Fig. 9. Positioning errors of the CDR's moving platform (a) before and (b) after actuation compensation with no loads

B. *Stiffness Characterization*

The CDR's stiffness was experimentally characterized. The moving platform was commanded to move to three representative positions at $[0\ 0\ -300\ \text{mm}]^T$ (#1), $[150\ \text{mm}\ 0\ -300\ \text{mm}]^T$ (#2) and $[0\ 75\ \text{mm}\ -400\ \text{mm}]^T$ (#3) all measured in $\{O\}$. The poses of reaching the three positions are shown in Fig. 11(a).

As shown in Fig. 11(b), a digital force gauge (HF-300 from Zhengkai Precision Instrument Co. China with a measurement range of ±300N) was used to push the CDR's moving platform. The gauge was driven by a power screw actuator with a lead of 2mm. The deflection would equal to the amount of pushed distance from the power screw, while the force was recorded by the force gauge. The forces v.s. the deflections in the XYZ directions are plotted in Fig. 11(c).

The CDR's stiffness varies from 0.80 N/mm to 3.75 N/mm in the XY directions, while the stiffness is from 33.17 N/mm to 57.55 N/mm in the Z direction. The stiffness in the Z direction is much higher, due to the fact that the continuum joint is inherently stiffer in its axial direction than in the lateral direction.

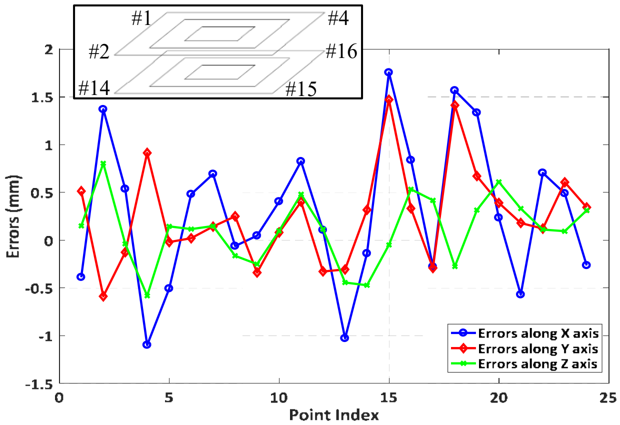

Fig. 10. Positioning errors for the additional 24 points

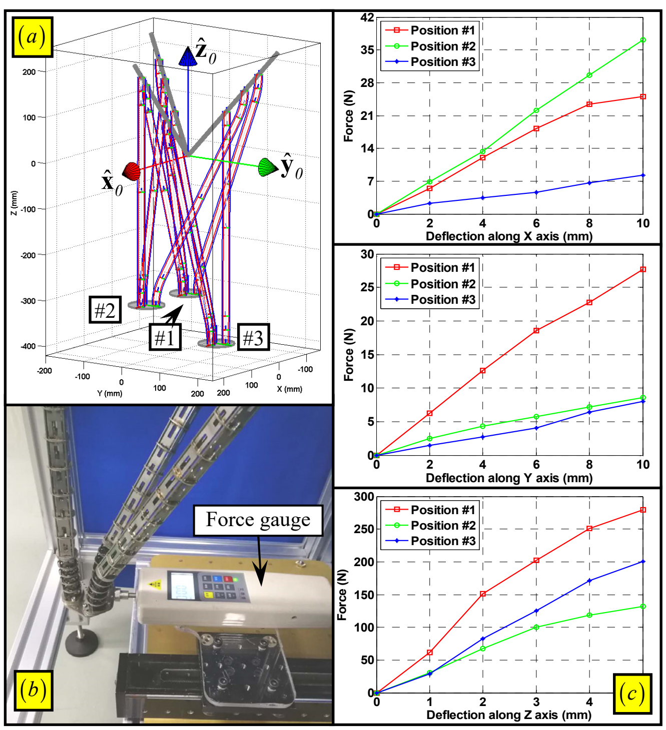

Fig. 11. Experiments for the stiffness characterizations: (a) the tested poses, (b) the setup, and (c) the results

C. *Movements of the CDR inside Its Workspace*

As the last set of experiments, the CDR was instructed to move to various positions inside its workspace to demonstrate the motion capability.

When a target position is given, for the ith leg of the CDR, the set of θ_i, δ_i and q_i values are solved from the kinematics in (5). The solutions are validated when the values are within the joint ranges (e.g., $\theta_i \in [0°, 90°]$ and $q_i \in [50\text{mm}, 300\text{mm}]$). Then $\mathbf{q} = [q_1\ q_2\ q_3]^T$ is obtained for the target pose.

A joint level interpolation was used to drive the CDR to accomplish a pick-and-place task. Movements of the CDR are shown in Fig. 12, as well as in the multimedia extension.

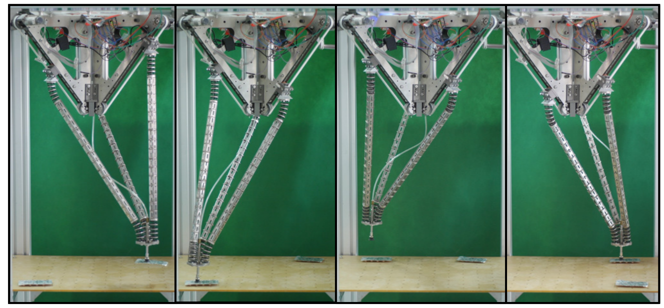
Fig. 12. The CDR's movements for a pick-and-place task

VI. Conclusions and Future Work

This paper proposes to design parallel robots with continuum joints. This attempt bridges continuum robots and parallel robots in a way different than the existing parallel continuum robots. To the best of the authors' knowledge, this development is the first of this kind.

Continuum joints bring the characteristics such as i) larger motion ranges and lower stiffness than those of universal or spherical joints, ii) simple kinematics stemmed from circular bending shapes, and iii) easily realizable coupling between two continuum joints via connecting the backbones. Larger motion ranges lead to larger workspace, while lower stiffness could avoid damaging delicate workpieces if this kind of robots is applied in pick-and-place tasks. Motion coupling between continuum joints introduces new possibilities of generating diverse movements.

As a illustrative example, the design concept, kinematics, system description and experimental characterizations of a Continuum Delta Robot (CDR) is presented in detail. The CDR is a 3-PCC robot where C designates a continuum joint. It is actuated by three guideway actuators and realizes three translational DoFs. After the motion calibration, the CDR realizes positioning accuracy of from $\pm$0.5 mm to $\pm$1.5 mm within its workspace. Its stiffness ranges from 3.75 N/mm in the XY directions to 57.55 N/mm in the Z direction.

The future work would be carried out mainly on two aspects. One is to further investigate possible forms of parallel robots with continuum joints. New design methodology would be developed to help synthesize new forms of this kind of parallel robots. One possibility is to change the arrangement of the guideway actuators to increase the isotropy of the stiffness. The other is to further the understanding of the proposed CDR, including i) investigating the forward and instantaneous kinematics, ii) introducing refined calibration processes for different bending of the continuum joints for improved positioning accuracy, iii) investigating its dynamic bandwidth for increased motion speeds, etc.

Acknowledgement

The authors thank Prof. Nabil Simaan and Prof. Pierre

Dupont for the discussions to properly name the proposed design and structure the manuscript.

REFERENCES

[1] G. Robinson and J. B. Davies, "Continuum Robots - A State of the Art," in *IEEE International Conference on Robotics and Automation (ICRA)*, Detroit, Michigan, 1999, pp. 2849-2853.

[2] I. D. Walker, "Continuous Backbone "Continuum" Robot Manipulators," *ISRN Robotics,* vol. 2013, No.726506, pp. 1-19, 2013.

[3] R. J. Webster and B. A. Jones, "Design and Kinematic Modeling of Constant Curvature Continuum Robots: A Review " *International Journal of Robotics Research,* vol. 29, No.13, pp. 1661-1683, Nov 2010.

[4] C. Shi, X. Luo, P. Qi, T. Li, S. Song, Z. Najdovski, T. Fukuda, and H. Ren, "Shape Sensing Techniques for Continuum Robots in Minimally Invasive Surgery: A Survey," *IEEE Transactions on Biomedical Engineering,* vol. 64, No.8, pp. 1665-1678, Aug 2017.

[5] C. Li and C. D. Rhan, "Design of Continuous Backbone, Cable-Driven Robots," *Journal of Mechanical Design,* vol. 124, pp. 265-271, 2002.

[6] K. Xu and N. Simaan, "Analytic Formulation for the Kinematics, Statics and Shape Restoration of Multibackbone Continuum Robots via Elliptic Integrals," *Journal of Mechanisms and Robotics,* vol. 2, No.011006, pp. 1-13, Feb 2010.

[7] D. C. Rucker and R. J. Webster, "Statics and Dynamics of Continuum Robots With General Tendon Routing and External Loading," *IEEE Transactions on Robotics,* vol. 27, No.6, pp. 1033-1044, Dec 2011.

[8] W. S. Rone and P. Ben-Tzvi, "Continuum Robot Dynamics Utilizing the Principle of Virtual Power," *IEEE Transactions on Robotics,* vol. 30, No.1, pp. 275-287, Feb 2014.

[9] J. Burgner-Kahrs, D. C. Rucker, and H. Choset, "Continuum Robots for Medical Applications: A Survey," *IEEE Transactions on Robotics,* vol. 31, No.6, pp. 1261-1280, Dec 2015.

[10] G. Immega and K. Antonelli, "The KSI Tentacle Manipulator," in *IEEE International Conference on Robotics and Automation (ICRA)*, Nagoya, Aichi, Japan, 1995, pp. 3149-3154.

[11] M. W. Hannan and I. D. Walker, "Kinematics and the Implementation of an Elephant's Trunk Manipulator and Other Continuum Style Robots," *Journal of Robotic Systems,* vol. 20, No.2, pp. 45-63, Feb 2003.

[12] T. Mahl, A. Hildebrandt, and O. Sawodny, "A Variable Curvature Continuum Kinematics for Kinematic Control of the Bionic Handling Assistant," *IEEE Transactions on Robotics,* vol. 30, No.4, pp. 935-949, Aug 2014.

[13] S. Liu, Z. Yang, Z. Zhu, L. Han, X. Zhu, and K. Xu, "Development of a Dexterous Continuum Manipulator for Exploration and Inspection in Confined Spaces," *Industrial Robot: An International Journal,* vol. 43, No.3, pp. 284-295, 2016.

[14] X. Dong, D. Axinte, D. Palmer, S. Cobos, M. Raffles, A. Rabani, and J. Kell, "Development Of a Slender Continuum Robotic System For On-Wing Inspection/Repair of Gas Turbine Engines," *Robotics and Computer-Integrated Manufacturing,* vol. 44, pp. 218-229, April 2017.

[15] I. D. Walker, R. Mattfeld, A. Mutlu, A. Bartow, and N. Giri, "A Novel Approach to Robotic Climbing Using Continuum Appendages in In-Situ Exploration," in *IEEE Aerospace Conference (AeroConf)*, Big Sky, Montana, USA, 2012, pp. 1-9.

[16] I. S. Godage, T. Nanayakkara, and D. G. Caldwell, "Locomotion with Continuum Limbs," in *IEEE/RSJ International Conference on Intelligent Robots and Systems (IROS)*, Vilamoura, Algarve, Portugal, 2012, pp. 293-298.

[17] C. E. Bryson and D. C. Rucker, "Toward Parallel Continuum Manipulators," in *IEEE International Conference on Robotics and Automation (ICRA)*, Hong Kong, China, 2014, pp. 778-785.

[18] A. L. Orekhov, C. B. Black, J. Till, S. Chung, and D. C. Rucker, "Analysis and Validation of a Teleoperated Surgical Parallel Continuum Manipulator," *IEEE Robotics and Automation Letters,* vol. 1, No.2, pp. 828-835, 2016.

[19] J. Till, C. E. Bryson, S. Chung, A. Orekhov, and D. C. Rucker, "Efficient Computation of Multiple Coupled Cosserat Rod Models for Real-Time Simulation and Control of Parallel Continuum Manipulators," in *IEEE International Conference on Robotics and Automation (ICRA)*, Seattle, Washington, 2015, pp. 5067-5074.

[20] J. Till and D. C. Rucker, "Elastic Stability of Cosserat Rods and Parallel Continuum Robots," *IEEE Transactions on Robotics,* vol. 33, No.3, pp. 718-733, 2017.

[21] M. Bouri and R. Clavel, "The Linear Delta: Developments and Applications," in *International Symposium on Robotics (ISR)*, Munich, Germany, 2010, pp. 1-8.

[22] L.-W. Tsai and S. Joshi, "Kinematic Analysis of 3-DOF Position Mechanisms for Use in Hybrid Kinematic Machines," *Journal of Mechanical Design,* vol. 124, No.2, pp. 245-253, 2002.

[23] D. Chablat and P. Wenger, "Architecture Optimization of a 3-DOF Translational Parallel Mechanism for Machining Applications, The Orthoglide," *IEEE Transactions on Robotics and Automation,* vol. 19, No.3, pp. 403-410, June 2003.

[24] Y. Li and Q. Xu, "Stiffness Analysis for a 3-PUU Parallel Kinematic Machine," *Mechanism and Machine Theory,* vol. 43, No.2, pp. 186-200, Feb 2008.

[25] J. P. Merlet, *Parallel Robots*, 2nd ed.: Springer, 2006.

[26] G. Piras, W. L. Cleghorn, and J. K. Mills, "Dynamic Finite-Element Analysis of a Planar High-Speed, High-Precision Parallel Manipulator With Flexible Links," *Mechanism and Machine Theory,* vol. 40, No.7, pp. 849-862, July 2005.

[27] J. E. McInroy, "Modeling and Design of Flexure Jointed Stewart Platforms for Control Purposes," *IEEE/ASME Transactions on Mechatronics,* vol. 7, No.1, pp. 95-99, Aug 2002.

[28] M. L. Culpepper and G. Anderson, "Design of a Low-Cost Nanomanipulator Which Utilizes a Monolithic, Spatial Compliant Mechanism," *Precision Engineering,* vol. 28, No.4, pp. 469-482, Oct 2004.

[29] H.-H. Pham and I.-M. Chen, "Stiffness Modeling of Flexure Parallel Mechanism," *Precision Engineering,* vol. 29, No.4, pp. 467-478, Oct 2005.

[30] C. Amici, A. Borboni, R. Faglia, D. Fausti, and P. L. Magnani, "A Parallel Compliant Meso-Manipulator for Finger Rehabilitation Treatments: Kinematic and Dynamic Analysis," in *IEEE/RSJ International Conference on Intelligent Robots and Systems (IROS)*, Nice, France, 2008, pp. 735-740.

[31] Y. Li and Q. Xu, "Design and Analysis of a Totally Decoupled Flexure-Based XY Parallel Micromanipulator," *IEEE Transactions on Robotics,* vol. 25, No.3, pp. 645-657, Mar 2009.

[32] C. Quennouelle and C. Gosselin, "Kinematostatic Modeling of Compliant Parallel Mechanisms," *Meccanica,* vol. 46, No.1, pp. 155-169, Feb 2011.

[33] K. Xu, J. Zhao, and M. Fu, "Development of the SJTU Unfoldable Robotic System (SURS) for Single Port Laparoscopy," *IEEE/ASME Transactions on Mechatronics,* vol. 20, No.5, pp. 2133-2145, Oct 2015.

[34] J. P. Merlet, "Solving the Forward Kinematics of a Gough-Type Parallel Manipulator with Interval Analysis," *The International Journal of Robotics Research,* vol. 23, No.3, pp. 221-235, March 2004.

[35] S. Nemat-Nassera and W.-G. Guo, "Superelastic and Cyclic Response of NiTi SMA at Various Strain Rates and Temperatures," *Mechanics of Materials,* vol. 38, No.5-6, pp. 463-474, May 2006.

[36] K. Xu and N. Simaan, "Actuation Compensation for Flexible Surgical Snake-like Robots with Redundant Remote Actuation," in *IEEE International Conference on Robotics and Automation (ICRA)*, Orlando, Florida, USA, 2006, pp. 4148- 4154.

[37] N. Simaan, K. Xu, A. Kapoor, W. Wei, P. Kazanzides, P. Flint, and R. H. Taylor, "Design and Integration of a Telerobotic System for Minimally Invasive Surgery of the Throat " *International Journal of Robotics Research,* vol. 28, No.9, pp. 1134-1153, 2009.

[38] P. Vischer and R. Clavel, "Kinematic Calibration of the Parallel Delta Robot," *Robotica,* vol. 16, No.2, pp. 207-218, March 1998.

[39] Y.-J. Chiu and M.-H. Perng, "Self-Calibration of a General Hexapod Manipulator with Enhanced Precision in 5-DOF Motions," *Mechanism and Machine Theory,* vol. 39, No.1, pp. 1-23, Jan 2004.

[40] D. Daney, N. Andreff, G. Chabert, and Y. Papegay, "Interval Method for Calibration of Parallel Robots: Vision-Based Experiments," *Mechanism and Machine Theory,* vol. 41, No.8, pp. 929-944, Aug 2006.